Available online at www.sciencedirect.com
ScienceDirect
Trans. Nonferrous Met. Soc. China 33(2023) 1906−1918
Transactions of Nonferrous Metals Society of China
www.tnmsc.cn

Evolution of passivating species on bornite surface during electrochemical dissolution

Mao-xin HONG[1,2], Hao LIN[1,2], Bao-jun YANG[1,2], Jing XIAO[1], Rui LIAO[1,2], Shi-chao YU[1,2], Chun-xiao ZHAO[1,2], Shi-tong LIU[1,2], Xin SUN[1,2], Jun WANG[1,2], Guan-zhou QIU[1,2]

1. School of Minerals Processing and Bioengineering, Central South University, Changsha 410083, China;
2. Key Laboratory of Biohydrometallurgy of Ministry of Education, Central South University, Changsha 410083, China

Received 7 February 2022; accepted 25 April 2022

Abstract: During bornite (bio)leaching, the relationship between the production of intermediate products and redox potential is unknown. In this study, a series of electrochemical tests and surface analytical methods were adopted to investigate the electrochemical dissolution of natural bornite and the formation of the sulfur species on the bornite surface. Electrochemical tests demonstrated that the surface of bornite experienced three distinct variations over a broad anodic potential (300−800 mV (vs Ag/AgCl)): "activation" (< 400 mV (vs Ag/AgCl)), "passivation" (400−700 mV (vs Ag/AgCl)), and "transpassivation" (> 700 mV (vs Ag/AgCl)). XPS results indicated that covellite-like species, S_n^{2-}/S^0, and insoluble SO_4^{2-} were considered as intermediate products during bornite electrochemical dissolution. Furthermore, AFM results proved that the accumulation of S_n^{2-}/S^0 made bornite surface suffer severe passivation when applied potentials were 600 and 700 mV (vs Ag/AgCl), respectively. The most advantageous potential for bornite (bio)leaching was shown to be 400 mV (vs Ag/AgCl).

Key words: bornite; bioleaching; electrochemical dissolution; surface species; atomic force microscope

1 Introduction

With the decline of readily mined copper deposits, processing/extraction challenges due to mineralogical complexity, poor grades, and very fine particles have become increasingly common in recent years [1]. The conventional copper beneficiation process faces a serious challenge as costs rise and environmental regulations become more stringent. (Bio)hydrometallurgy, which is a relatively simple, low-cost, and environmentally friendly technology, has gotten a lot of attention and has been used to process low-grade and complex copper sulfide minerals successfully [2−4]. Previous research on the (bio)hydrometallurgy of copper resources has mostly focused on chalcopyrite [5,6]. However, owing to the facile passivation of mineral surfaces in the ferric sulfate system and the high binding energy, effective copper extraction from chalcopyrite remains a challenge [7,8]. Other copper sulfide minerals, on the other hand, have received less attention.

Bornite (Cu_5FeS_4), a widely dispersed copper mineral with commercial significance, is also important [9]. Though bornite is simpler to dissolve in the acidic system due to its lower lattice energy than chalcopyrite, the exact dissolving mechanism is still debated because the characteristics of intermediate products generated during the leaching process differ. It was reported that bornite was oxidized by two steps in acidic ferric sulfate solution [10]. In the first stage of dissolution, some non-stoichiometric copper products were considered to form, such as Cu_3FeS_4 [10], $Cu_{2.5}FeS_4$ [11], $CuFeS_2$ [12], and CuS [13]. Additionally, the copper

Corresponding author: Jun WANG, Tel: +86-731-88876557, E-mail: wjwq2000@126.com
DOI: 10.1016/S1003-6326(23)66231-4

extraction of bornite is considerable in the presence of bacteria [14,15]. However, the intermediates in the bornite bioleaching process were more complicated, and the non-stoichiometric copper products like $Cu_9Fe_9S_{16}$ and $CuFe_2S_3$ were also detected [14,16].

Furthermore, certain products, such as elemental sulfur and jarosite, are thought to develop on the surface of the bornite in the late stages of bioleaching, potentially impeding further dissolution. BEVILAQUA et al [17,18] certified an elemental sulfur film formed on the bornite surface during (bio)leaching, according to results of cyclic voltammetry and electrochemical impedance spectroscopy. Similarly, a considerable number of elemental sulfur peaks were identified on XRD patterns of bornite residues leached by *Leptospirillum ferriphilum* and *Acidithiobacillus caldus* [14]. According to the results of synchrotron XRD in the research of WANG et al [16], jarosite was discovered in addition to elemental sulfur, with the formation of jarosite appearing to have no effect on the dissolution of bornite. ZHAO et al [19] proposed that CuS, FeOOH, and elemental sulfur were found on the surface of bornite during bioleaching in the presence of moderately thermophilic microorganisms (*L. ferriphilum* and *A. caldus*). Therefore, the presence of a sulfur-rich film may play a major role in preventing bornite (bio)leaching, according to these findings. In fact, redox potential (ORP) has a significant impact on the dissolution of copper sulfide minerals like chalcopyrite [20]. Chalcopyrite, for example, likes to be reduced to produce chalcocite, which is simpler to dissolve at low redox potential, but jarosite prefers to form on the surface of chalcopyrite at a high ORP, obstructing chalcopyrite dissolution [21]. However, it should be noted that previous investigations have overlooked the link between the generation of intermediate products and redox potential during the (bio)leaching of bornite.

Therefore, in order to fill this knowledge gap, this study aimed to identify the relationship between redox potential and the formation of intermediate products on bornite surface in bornite (bio)leaching process via electrochemical methods. A series of electrochemical tests were carried out over a broad anodic potential range (300−800 mV (vs Ag/AgCl)), and the formation of the intermediate products on the bornite surface was investigated with XPS and AFM.

2 Experimental

2.1 Bornite samples

Bornite samples were collected from Yushui Copper Mine, Guangdong Province, China, which contained 62.72 wt.% Cu, 11.72 wt.% Fe, 23.83 wt.% S (Table 1) by chemical element analysis. The result of XRD indicated that bornite samples were of high purity (Fig. 1). Bornite samples were cut into cylinders with a diameter of about 1.2 cm and a thickness of 0.5 cm, then polished using silicon carbide paper (5 μm) in order to remove the surface oxides and obtain a smooth surface prior to each electrochemical experiment. The exposed surface of the bornite electrode to the electrolyte was around 1 cm^2.

Table 1 Chemical composition of bornite sample (wt.%)

Cu	Fe	S	Ag	Cl	Ca	Co	Ni	Zn	Pb
62.72	11.72	23.83	1.07	0.02	0.03	0.04	0.02	0.32	0.23

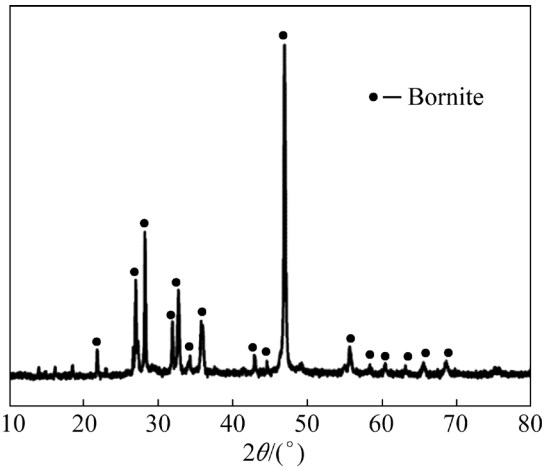

Fig. 1 XRD pattern of bornite sample

2.2 Electrochemical experiments

A conventional three-electrode cell was used to perform the electrochemical experiments. A double-wall glass reactor with an effective volume of 500 mL was used as the electrochemical cell. Graphite rods were used as counter electrodes, and Ag/AgCl (3.0 mol/L KCl) electrode was used as the reference electrode. The electrolyte was the

iron-free 9K medium containing 3 g/L $(NH_4)_2SO_4$, 0.5 g/L K_2HPO_4, 0.5 g/L $MgSO_4·7H_2O$, 0.01 g/L $Ca(NO_3)_2$ and 0.1 g/L KCl [22]. And the pH of the electrolyte was adjusted to 2.0 with 1 mol/L sulfuric acid, which was the favorable pH for most leaching bacteria like *A. ferrooxidans* [23] and the most commonly reported initial pH value in bioleaching process [24,25]. Nitrogen gas was sparged for 20 min prior to electrochemical experiments to remove dissolved oxygen from the electrolyte. All electrochemical experiments were performed with the Princeton Model 283 potentiostat (EG & G of Princeton Applied Research) coupled with a personal computer.

Bornite electrodes were immersed in the electrolyte for 30 min before each experiment to ensure the repeatability and stability of the electrochemical experiments. Cyclic voltammetry (CV), linear sweep voltammetry (LSV), chrono-amperometry (CA), Tafel tests, and electrochemical impedance spectroscopy (EIS) were carried out in the electrochemical experiments. The CV test was performed at a scan rate of 200 mV/s from OCP to 800 mV, and then reversed to −800 mV for four cycles. The LSV test was conducted at a scan rate of 10 mV/s from OCP to 1.00 V. The CA tests were proceeded at the potentials of 300, 400, 500, 600, 700, and 800 mV and maintained for 6 h. Tafel experiments were performed after CA tests with a sweep rate of 2 mV/s. The EIS experiments were performed after CA tests at an amplitude of 50 mV in the frequency range from 10^{-1} to 10^5 Hz, and the software of ZSimpwin 3.20 (2004) was used to fit EIS data.

All the electrode potential values reported in this work were in respect to Ag/AgCl reference electrode. The process of working electrodes preparation and electrochemical measurements was presented in Fig. 2.

2.3 Surface characterization

After electrochemical experiments, bornite electrodes were rinsed with distilled water and ethyl alcohol several times and then transferred to a vacuum oven and dried at 45 °C. Afterwards, the dried samples were investigated by XPS (ESCALAB 250Xi, Thermo Fisher Scientific, Waltham, MA, USA). XPS data were recorded at the constant pass energy of 20 eV and 0.1 eV/step with Al K_α X-ray source. Calibration was to use the C 1s binding energy at 284.8 eV. Due to spin-orbit splitting, the 2p peaks of Cu and S existed in the form of a double-peak (Cu/S $2p_{3/2}$ and Cu/S $2p_{1/2}$), and the peak intensity of $2p_{3/2}$ was twice the intensity of the $2p_{1/2}$ peak. The splitting energy of the spin-orbit doublets of Cu and S was 19.9 and 1.2 eV, respectively. The Gaussian–Lorentzian (SGL) function was used for fitting the Cu and S 2p spectra. The background fitting was performed using the Smart method. In order to simplify the graph, only the S $2p_{3/2}$ peaks were shown in the high-resolution XPS results of S 2p spectra. Atomic force microscope (MultimodeV, Veeco Metrology, USA) was used to observe the variation of the surface of bornite electrode after treating with different applied potentials, with a test area of 5 μm × 5 μm for each group of samples. The NanoScope Analysis software was used to analyze the microscopic morphology and surface roughness data.

3 Results and discussion

3.1 Electrochemical behavior of bornite electrodes in iron-free 9K medium

Figure 3(a) depicts CV curves of a freshly polished bornite electrode in iron-free 9K culture medium with pH=2.0 via a positive scan route. During the anodic scan, four peaks (labeled as e, f,

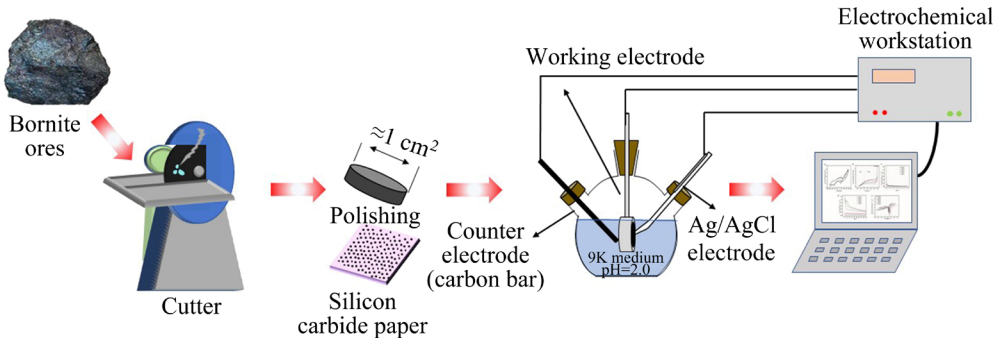

Fig. 2 Illustration of working electrode preparation and electrochemical measurement

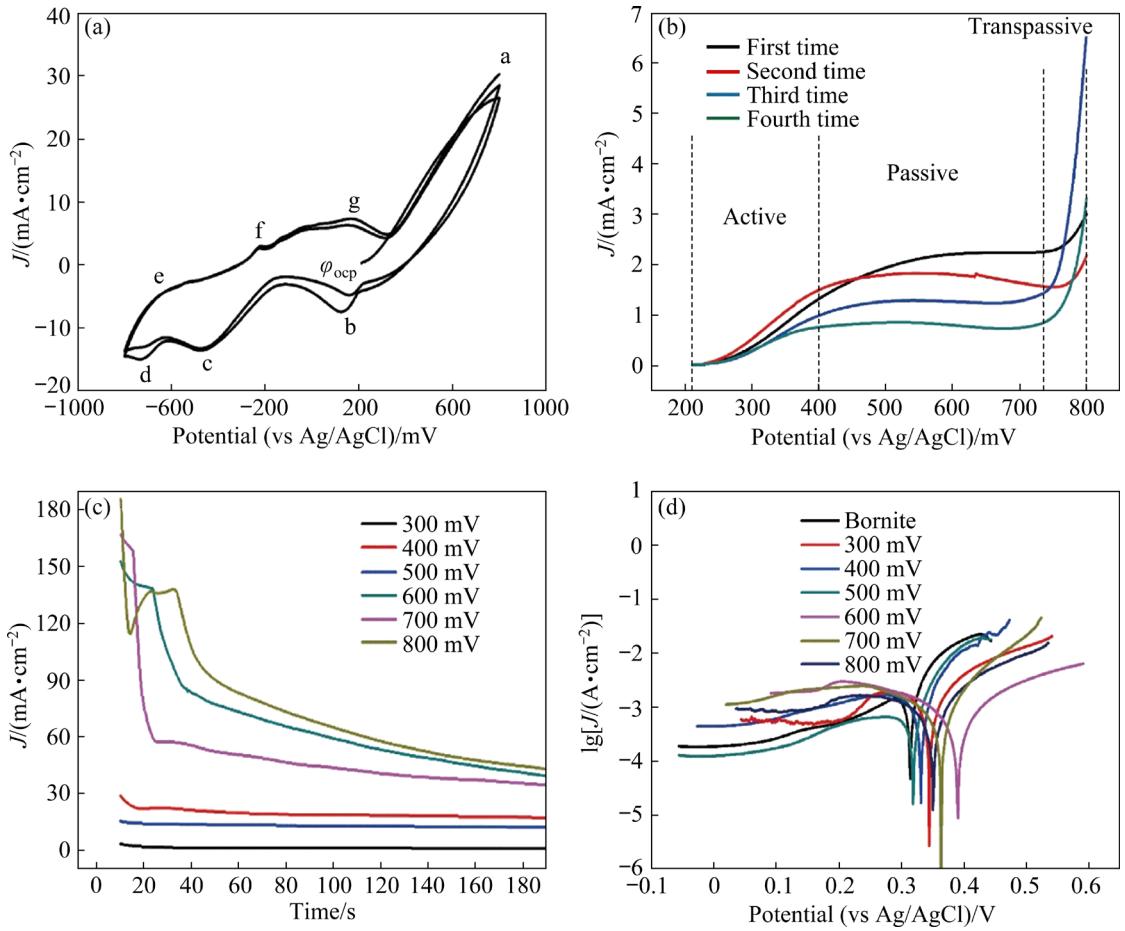

Fig. 3 CV curves of natural bornite electrodes (a), LSV results of bornite electrodes tested 4 times (b), chronoamperometry curves of bornite electrodes held at various anodic potentials for the first 180 s in electrolyte (c), and Tafel plots of bornite electrodes applied with different potentials (d)

g and a) were identified at potentials of −650, −200, 200 and 800 mV, respectively. Peak e was mainly related to the oxidation of copper (Reaction (1)) [16,26]. Peak f was related to the oxidation of chalcocite formed in the potential region of Peak e (Reactions (2) and (3)) [16]. Peak g represented the oxidation of Fe^{2+} to Fe^{3+} (Reaction (4)), which was a reverse reaction related to Peak b. Peak a in the range from 600 to 800 mV was attributed to the oxidation process of bornite and the formation of covellite (Reactions (5)−(7)) [27]. In the reverse scan from 800 to −800 mV, it is obvious that three peaks (b, c and d) were detected at around 150, −450 and −700 mV, respectively. Peak b was reported as the reduction of ferric ions, copper ions and elemental sulfur (Reactions (8) and (9)) [28]. It should be noticed that the cathodic Peak b shifted towards negative potentials in the second round of scanning, which meant a decrease in reversibility [29]. And it was possibly related to the formation of oxidation products from Peak a, such as CuS and S^0, which might hinder the electron transfer. Peak c was in relation to the reduction of covellite (Reaction (10)) [30]. And Peak d could be associated with the reduction of chalcocite to metallic copper (Reaction (11)) [17], which was the reversible electrode process of Peak e.

$$2Cu^0+H_2S=Cu_2S+2H^++e \quad (1)$$

$$Cu_2S=Cu_{2-x}S+xCu^{2+}+2xe \quad (2)$$

$$Cu_{2-x}S=CuS+(1-x)Cu^{2+}+2(1-x)e \quad (3)$$

$$Fe^{2+}=Fe^{3+}+e \quad (4)$$

$$Cu_5FeS_4=Cu_{5-x}FeS_4+xCu^{2+}+2xe \quad (5)$$

$$Cu_{5-x}FeS_4+6H^+=CuS+(4-x)Cu^{2+}+3H_2S+Fe^{3+}+(5-2x)e \quad (6)$$

$$Cu_{5-x}FeS_4=(5-x)Cu^{2+}+4S^0+Fe^{3+}+(13-2x)e \quad (7)$$

$$Fe^{3+} + e = Fe^{2+} \quad (8)$$

$$Cu^{2+} + S^0 + 2e = CuS \quad (9)$$

$$2CuS + 2H^+ + 2e = Cu_2S + H_2S \quad (10)$$

$$Cu_2S + 2H^+ + 2e = 2Cu^0 + H_2S \quad (11)$$

LSV curves of one bornite electrode tested four times are shown in Fig. 3(b). The surface of bornite electrode was re-polished before each test. The differences between four curves could be due to the impurity elements in bornite lattice (Table 1) and polished surface, which might have a certain effect on the conductivity. However, three regions were evidently observed from OCP to 800 mV in all curves. Specifically, current density increased rapidly in the applied potential range from OCP to 400 mV, indicating that the dissolution of bornite at this potential was rapid. As a result, it was considered as the active region [31]. Afterward, the current density of the bornite electrode remained constant throughout a wide range of potentials (400−740 mV), and it should be considered as the passive region for the rate-limiting stage of bornite (bio)leaching. Because the potential was insufficient to transport oxidation products through the sulfur-rich layer in this location, i.e., current density was unaffected by potential [32]. In this applied potential range, most studies found the development of intermediate products like elemental sulfur and jarosite that would hinder further dissolution of bornite [14,19]. The current density increased suddenly when the potential surpassed 740 mV, and the transpassive phenomenon developed.

The passivation of bornite surface occurred primarily at higher potentials, according to the results of CV and LSV tests. As a result, CA experiments were carried out to support this finding. The bornite electrodes were tested for 6 h at potentials of 300, 400, 500, 600, 700, and 800 mV, and the results of the first 180 s with the most obvious change are shown in Fig. 3(c). The current density dropped in varying degrees over six applied potentials. Minor decrease was observed in current density for bornite electrodes with polarized potentials of 300, 400 and 500 mV in the first 180 s, meaning that the passivation was relatively weak under these potentials. The initial current density at 500 mV was smaller than that at 400 mV, which meant that the surface of bornite started to passivate. The current density reduced from 150 to 130 mA/cm^2 in the first 20 s at 600 mV, and then dropped rapidly to 90 mA/cm^2 at about 30 s. The shift in current density at 700 mV in the first 17 s was more rapid, which was responsible for the decreased electron transfer on the bornite surface. Despite the fact that the current density at 800 mV dropped in the first 5 s, it plateaued at 120 mA/cm^2. This meant that a thinner coating formed on the bornite surface at 800 mV than that at 700 mV, which was compatible with LSV results. The formation of the passivation film on the surface of bornite electrodes may be responsible for the decline of current density [16], preventing electrons from diffusing into the bulk of mineral [33]. Thus, Tafel and electrochemical impedance spectroscopy (EIS) tests were performed after CA testing to further study the changes in electrochemical characteristics on the surface of bornite after polarizing with various potentials and verify the control step of electron transfer.

Figure 3(d) shows the Tafel curves of bornite electrodes applied with various potentials. Based on the data in Fig. 3(d) and using the method of Tafel extrapolation, the electrochemical parameters can be obtained. Table 2 presents the detailed parameters of the polarization resistance (R_p) and corrosion current density (J_{corr}) of bornite electrodes. Over the applied potential range from 300 to 800 mV, the bornite electrode with the treated potential of 400 mV showed the lowest R_p and the greatest J_{corr} (Table 2), indicating that bornite was favorably oxidized at this potential. Similarly, it was reported that the copper extraction of bornite increased rapidly during bioleaching when solution redox potential (ORP) increased in the range from 360 to 450 mV [16,34], which was in accordance with the results in this study. Additionally, there was a decline in J_{corr} of polarized electrodes from

Table 2 Results of Tafel tests

Sample	R_p/(Ω·cm^2)	J_{corr}/(mA·cm^{-2})
Original bornite	8.321	5.703
300 mV	26.282	2.207
400 mV	11.406	3.297
500 mV	21.234	2.517
600 mV	39.903	1.204
700 mV	27.817	1.351
800 mV	25.300	2.061

400 to 600 mV, which was compatible with the passive region concluded by the results of LSV tests. Then, a noticeable increase in J_{corr} confirmed that the surface of the bornite electrode was transpassivated.

Figure 4 presents the experimental and simulated Nyquist plots of original bornite and bornite electrodes polarized. For all of them, there were two incomplete semicircles in the high and intermediate frequency regions (Figs. 4(a−g)). The high-frequency semicircle was related to the reduction of Fe(III) to Fe(II), while semicircle in intermediate frequency regions was ascribed to the oxidation on the bornite surface [17,35]. In the low-frequency region, there was a straight line with a typical Warburg impedance (W), which was related to the existence of a finite diffusion process [36]. The equivalent circuit corresponded to $R_s(Q_1(R_1))(Q_2(R_2W))$ (Fig. 4(i)). The fitting parameters for all model circuits of bornite electrodes at different anodic potentials are provided in Table 3. The range of all the χ^2 values was in the order of 10^{-4}, indicating a good fit between the experimental data and the equivalent circuit models. R_s and R_1 represented the electrolyte resistance and the charge transfer resistance during the oxidation of bornite, respectively. R_2 referred to the charge transfer resistance during the oxidation of surface film, which was determined by the electrochemical reaction rate on the bornite electrode. Q_1 and Q_2 represented the double-film capacitances between electrode/electrolyte and passive film/electrolyte, respectively [37]. It could be seen that R_1 and R_2 of bornite electrodes polarized with 600 and 700 mV were extremely higher than others (Fig. 4(h)), which indicated that a compact passivation layer was formed on the surface of bornite. And values of R_2 were substantially higher than those of R_s and R_1 (Table 3), indicating that the formation of surface layer was the main factor affecting the oxidation of bornite and the control step was the electron transfer. The value of R_2 was the smallest with 164.900 Ω·cm^2 at an applied potential of 400 mV,

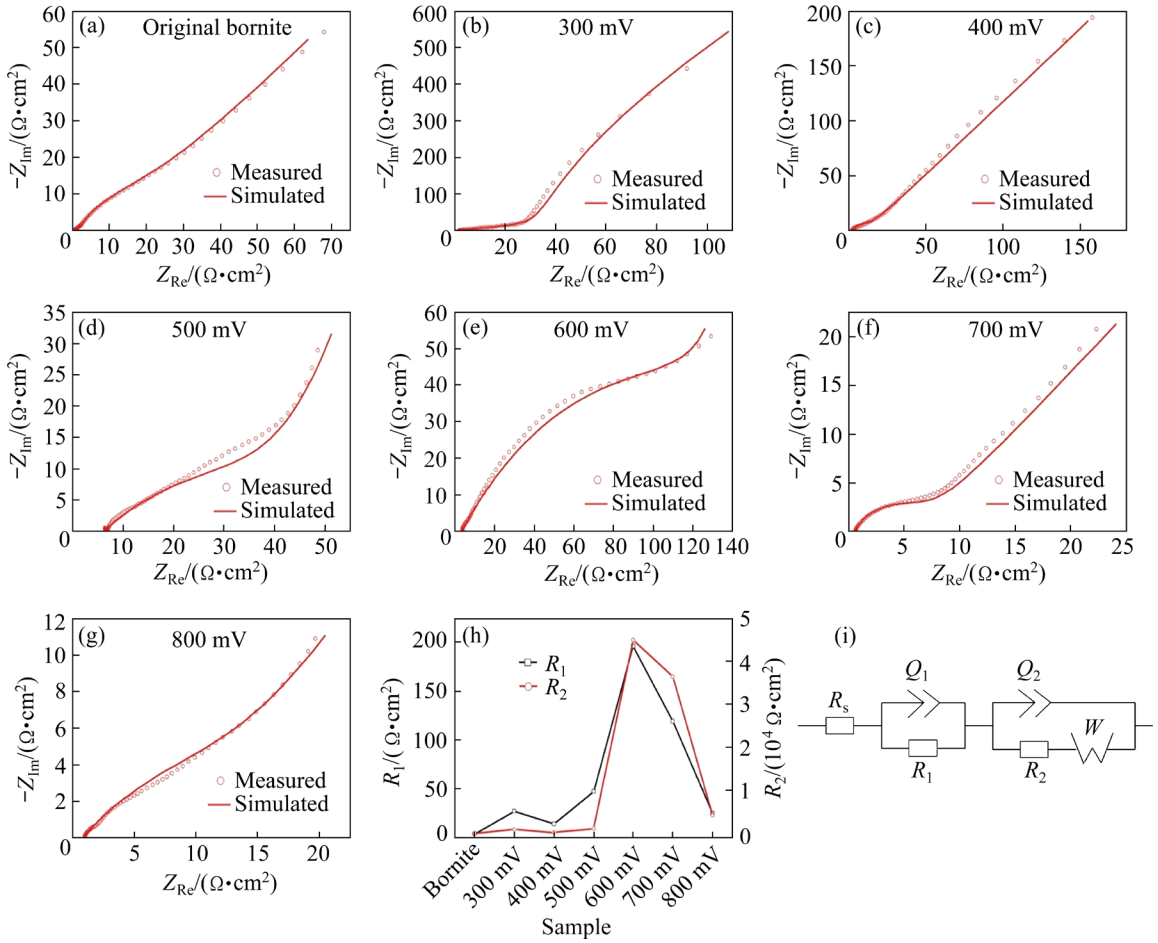

Fig. 4 Impedance diagrams of original bornite (a) and bornite electrodes applied with different anodic potentials (300−800 mV) (b−g), variations in R_1 and R_2 (h), and equivalent circuit (i)

Table 3 Fitting parameters of equivalent circuit

Sample	R_s/ ($\Omega\cdot cm^2$)	$Y_{0,1}$/ ($10^{-3}S\cdot s^n\cdot cm^{-2}$)	R_1/ ($\Omega\cdot cm^{-2}$)	R_2/ ($\Omega\cdot cm^2$)	$Y_{0,2}$/ ($10^{-3}S\cdot s^n\cdot cm^{-2}$)	W/ ($10^{-1}S\cdot s^{0.5}\cdot cm^{-2}$)	χ^2/ 10^{-4}
Original bornite	1.547	149.300	3.706	8.900	6.401	0.441	6.130
300 mV	1.959	6.000	26.940	942.000	26.320	0.014	8.770
400 mV	1.884	2.456	14.310	164.900	197.500	0	7.620
500 mV	6.199	2.044	47.600	1122.123	356.700	0	9.670
600 mV	1.622	11.180	196.100	44890.000	357.400	0.120	7.560
700 mV	0.602	6.667	119.114	36480.000	10.980	0	8.320
800 mV	0.789	49.860	24.889	4228.000	177.602	0	6.330

$Y_{0,1}$ is the fitting parameter of Q_1; $Y_{0,2}$ is the fitting parameter of Q_2; χ^2 is the Chi-squared value of the fitted equivalent circuit

which meant barely passivated film formed at this potential, and it was consistent with the bioleaching results of our previous studies [14,34,38]. There was a significant rise observed in R_2 when the anodic potentials of 600 mV (44890.000 $\Omega\cdot cm^2$) and 700 mV (36480.000 $\Omega\cdot cm^2$) were applied on the bornite surface, which was more than 200 times higher than that at 400 mV. This meant that the formation of the passivated film on the bornite surface severely hindered the charge transfer. At the applied potential of 800 mV, R_2 rapidly dropped to 4228.000 $\Omega\cdot cm^2$, representing that the passivation was diminished.

3.2 Characterization of intermediate products on bornite surface

Cu 2p spectra of the original bornite and polarized electrodes are shown in Fig. 5. The binding energy range of Cu $2p_{3/2}$ for cuprous (Cu^+) compounds was 932.0−932.9 eV, while for cupric (Cu^{2+}) compounds, the binding energy was from 933.1 to 936.6 eV [39]. In addition, there was no shake-up satellite peak between 940 and 950 eV, indicating that Cu was present in the form of Cu(I) in all bornite electrodes [40,41]. As for the original bornite, Cu $2p_{3/2}$ and Cu $2p_{1/2}$ peaks were located at 932.0 and 951.9 eV, respectively, which corresponded to the Cu(I)−S in bornite bulk (Fig. 5(a)). After polarization on bornite surface, a slight shift in Cu $2p_{3/2}$ peak was observed from 932.0 to 932.4 eV, which meant that a new copper monovalent compound was formed on the surface of bornite. And the possible substance with Cu $2p_{3/2}$ at 932.4 eV was contributed to covellite-like species (CuS) [39]. In addition, the Cu LMM peaks of polarized electrodes were located at 568.7, 568.7, 568.8, and 568.9 eV, respectively, which were

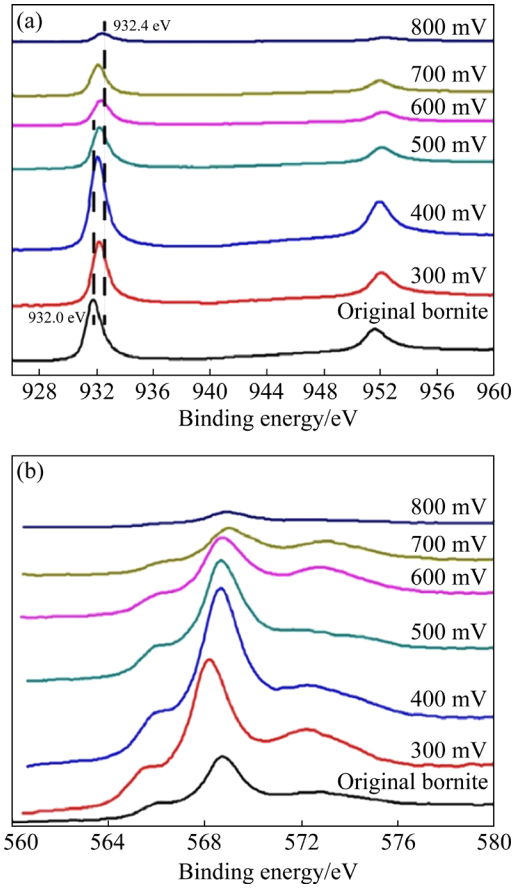

Fig. 5 Cu 2p (a) and Cu LMM (b) XPS spectra of original and polarized bornite electrodes

previously reported as Cu LMM peaks of CuS (Fig. 5(b)) [42]. The formation of CuS was considered as one of the intermediate products that would hinder the dissolution of bornite [43]. It was worth noticing that intensity of Cu $2p_{3/2}$ peaks showed an upward trend from 300 to 400 mV, followed by a downward trend from 400 to 800 mV, confirming that the surface of bornite suffered activation and then passivation at different anodic potentials.

The S $2p_{3/2}$ XPS spectra and contents of sulfur species on bornite surface are presented in Fig. 6. Two evident peaks with binding energies at 161.3 and 162.4 eV were observed in the original bornite (Fig. 6(a)). The strongest S $2p_{3/2}$ peak at 161.3 eV was ascribed to S^{2-} in the bulk of bornite [44], and the other peak with lower intensity at 162.4 eV was assigned to the surface S_2^{2-}, which was predominantly associated with slight oxidation on bornite surface [19]. On the spectra of polarized electrodes, a newly found S $2p_{3/2}$ peak at 163.8 eV was clearly visible (Figs. 6(b−g)). According to previous studies, this peak was consistent with the reported elemental sulfur (163.05−164.7 eV) or polysulfide (163.0−163.9 eV) [45]. Polysulfide was hard to achieve differential fit due to its multiple substances with different chain lengths [14]. As a result, the S $2p_{3/2}$ peak in the binding energy range from 163.0 to 164.7 eV was attributed to S_n^{2-}/S^0 in this study. Additionally, S $2p_{3/2}$ peak with slight intensity at a binding energy of 168.5 eV started to appear from 300 to 800 mV. S $2p_{3/2}$ peaks in the binding energy range of 168.0−169.0 eV were reported to represent SO_4^{2-} [46]. However, insoluble sulfate was not identified on bornite surface at potentials from 300 to 650 mV in the electrochemical research work of ZHAO et al [19]. The appearance of insoluble SO_4^{2-} was mostly due to the formation of jarosite ($KFe_3(SO_4)_2(OH)_6$) for a trace amount of dissolved oxygen and potassium

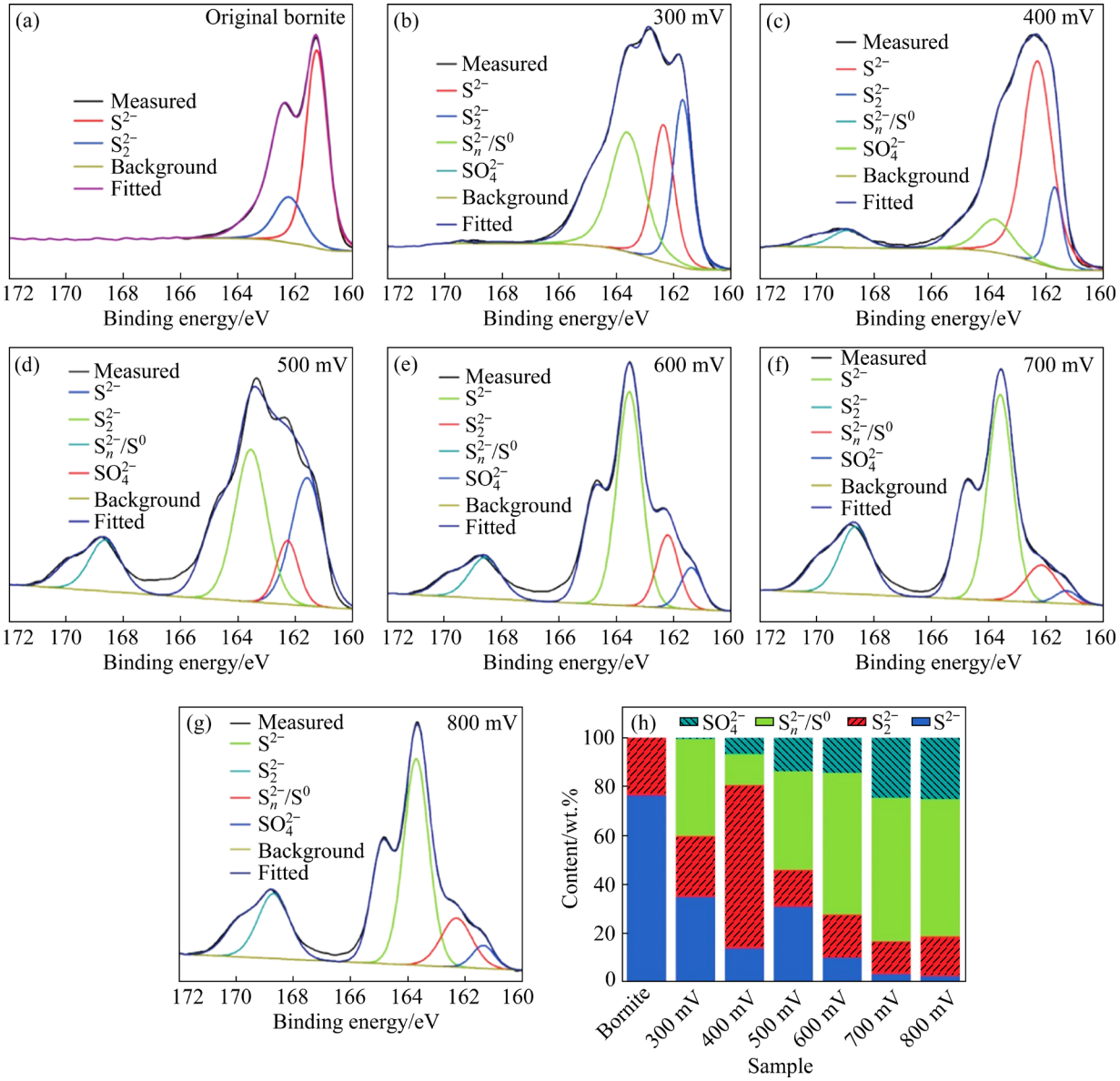

Fig. 6 S $2p_{3/2}$ XPS spectra of original bornite (a) and bornite electrodes polarized at 300, 400, 500, 600, 700 and 800 mV, respectively (b−g), and contents of sulfur species on surface of bornite electrodes after polarization (h)

existed in the electrolyte of the iron-free 9K medium [47]. In addition, S_n^{2-}/S^0 and insoluble SO_4^{2-} (primarily jarosite) were also recognized as possible passivating substances that would generate during the bioleaching of bornite [48]. It is worth noting that the intensities of the S_n^{2-}/S^0 and SO_4^{2-} of the bornite electrode with applied potential of 400 mV were the lowest (Fig. 6(c)), which indicated that sulfur-rich layer was scarcely generated on the surface at this point. This finding was consistent with the result of EIS. As a result, the oxidation of bornite at this potential was easy to achieve.

As shown in Fig. 6(h), clearly, sulfur species on bornite electrode with applied potential of 400 mV was predominantly S_2^{2-} (more than 60%), which could be attributed to the appearance of intermediate products like CuS. As mentioned above, it was reported that bornite dissolved rapidly in the first stage, which would end up with the production of CuS (Reaction (6)) [10]. In other words, the conversion of bornite to internal covellite-like species was related to the rapid dissolution of bornite. Thus, 400 mV was the favorable potential for rapid dissolution of bornite. When the applied potential was higher than 400 mV, the proportion of SO_4^{2-} was increased (Fig. 6(h)), which was consistent with the finding that jarosite was prone to be produced at high solution potential during bioleaching [24]. Despite the presence of jarosite on the surface of polarized bornite electrodes, S_n^{2-}/S^0 accounted for over half of the total sulfur species from 500 to 800 mV. As a result, the primary sulfur-rich layer generated on the bornite surface at high anodic potential could be concluded as S_n^{2-}/S^0, which was in agreement with the results of bioleaching experiments in previous studies [14,19].

3.3 Morphology of sulfur-rich layer formed on bornite surface at different potentials

Microscopic morphology images of the original bornite and polarized electrodes were analyzed using an atomic force microscope (AFM). The top views and three-dimensional schematics are shown in Fig. 7. Scratch flaws were visible on the surfaces of bornite electrodes in the detection range of 5 μm × 5 μm, owning to the polishing prior to electrochemical tests. The surface of the original bornite had minor scratches and clear boundaries, while it became rougher after being treated with different potentials in addition to 400 mV, indicating that bornite surface suffered passivation to a varying degree. In addition, the surface roughness of bornite electrodes was analyzed using software called NanoScope Analysis, and the surface roughness was related to the height difference of the selected points. Four smoother locations (*a*, *b*, *c*, and *d*) with equal areas were

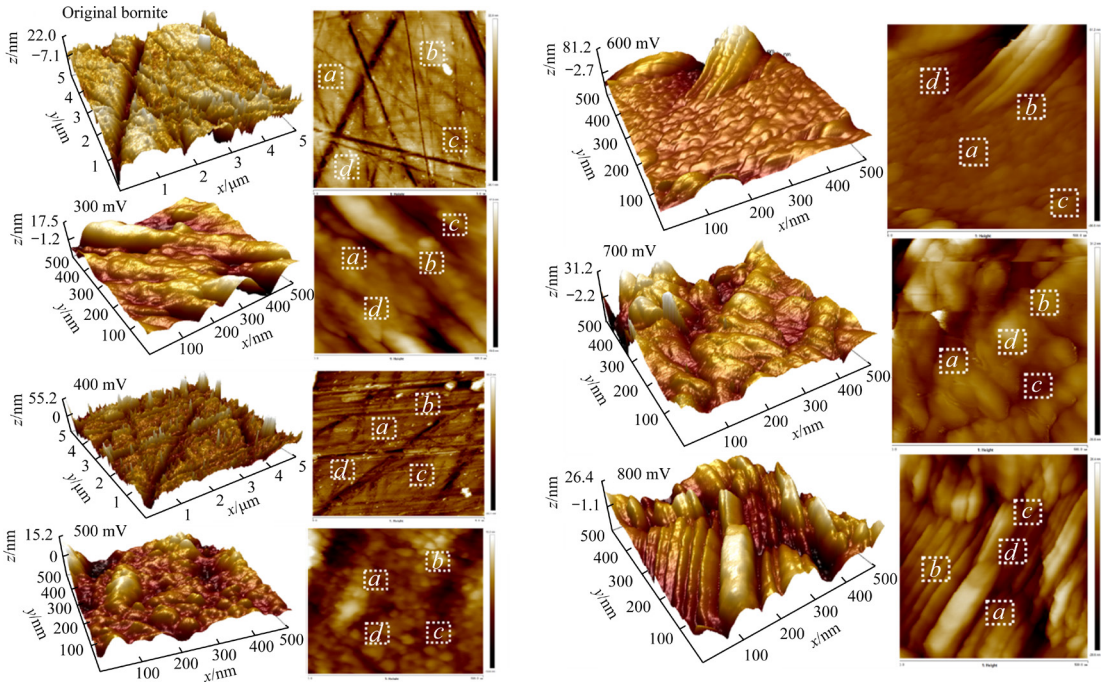

Fig. 7 AFM images of original bornite and polarized bornite electrodes

selected in each set of tests to eliminate errors caused by surface flaws, and the full parameters of surface roughness on bornite were provided in Table 4. It is clear that bornite electrodes treated with 400 and 700 mV had the smallest and the largest average values with 1.240 and 1.714 nm, respectively, which confirmed that the passivation layer became thicker in this potential range. According to the results of XPS of S 2p, the passivation layer primarily consisted of S_n^{2-}/S^0. Therefore, it is vital to control solution redox potential at low level during bornite (bio)leaching. Some methods were reported to be effective on ORP control during (bio)leaching process, such as adding pyrite [2,49] and using microcontroller technology [50].

Table 4 Surface roughness of original and polarized bornite electrodes (nm)

Sample	*a*	*b*	*c*	*d*	Average value (*a*, *b*, *c* and *d*)	Full area average value
Original bornite	1.024	1.007	1.214	1.227	1.118	1.196
300 mV	1.169	1.224	1.275	1.368	1.259	1.310
400 mV	1.162	1.253	1.326	1.139	1.220	1.240
500 mV	1.321	1.315	1.240	1.324	1.325	1.563
600 mV	1.414	1.445	1.212	1.377	1.362	1.616
700 mV	1.240	1.377	1.229	1.250	1.274	1.714
800 mV	1.306	1.243	1.221	1.392	1.291	1.680

3.4 Proposed model for interpreting passivation process on bornite surface during (bio)-leaching

According to the above results, a proposed model for interpreting passivating products formed on bornite surface during (bio)leaching is provided in Fig. 8. Bornite is a natural semiconductor, and the dissolution of bornite during leaching can be recognized as an electrochemical dissolution. The presence of leaching bacteria can catalyze the dissolution of bornite without changing the dissolution mechanism [14]. During the bioleaching of bornite, the solution ORP will gradually increase because the releasing Fe^{2+} will be oxidized to Fe^{3+} by ferrous-oxidizing bacteria. Under low ORP (<300 mV), the dissolution of bornite is limited due to the limitation of electron transfer from bornite surface to Fe^{3+}/Fe^{2+} couple (the main redox couple in bioleaching) [19]. When OPR increases to around 400 mV, bornite is favorable to dissolve to form CuS [19,48]. As the potential continues to rise (400−700 mV), S^0/S_n^{2-} will be accumulated on the surface of bornite, which will weaken the charge transfer and lead to passivation. Jarosite will also generate in this potential range, owning to further oxidation of polysulfides. Though there will be transpassivation when the potential reaches 800 mV, it is impossible to achieve in conventional bioleaching conditions. Therefore, it is vital to control ORP at a low level during bornite bioleaching to avoid the formation of large amounts of S^0/S_n^{2-}.

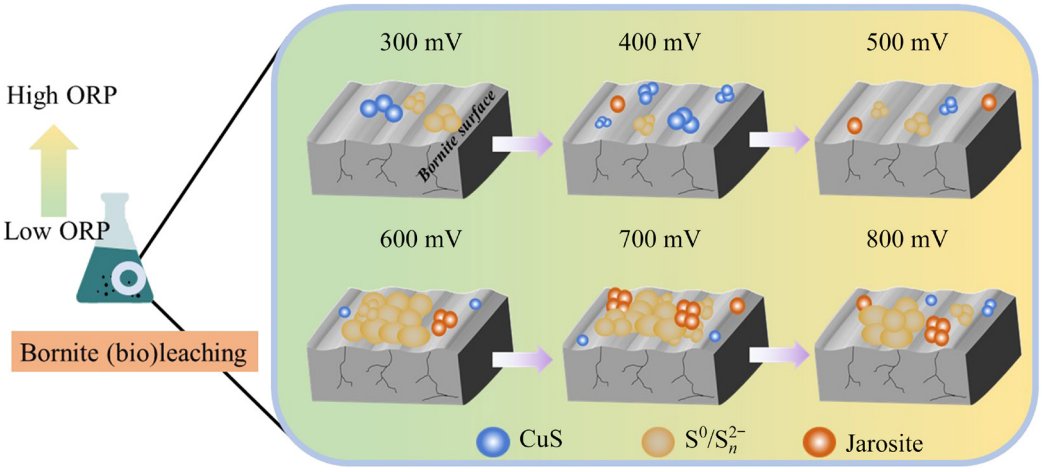

Fig. 8 Proposed model for interpreting intermediate products formed on bornite surface during (bio)leaching at different redox potentials

4 Conclusions

(1) The electrochemical dissolution of bornite over a broad anodic potential range (300−800 mV) could be divided into three parts, i.e., activation (< 400 mV), passivation (400−700 mV), and transpassivation (>700 mV) referring to different anodic potentials. Specifically, the bornite surface suffered severe passivation when applied potentials were 600 and 700 mV.

(2) The XPS results of Cu 2p indicated that covellite-species were formed on bornite surface. The S $2p_{3/2}$ spectra proved that S^{2-} converted to S_2^{2-}, S_n^{2-}/S^0, and SO_4^{2-} with potential increasing, and the severe passivation on the bornite surface at high anodic potential was caused by S_n^{2-}/S^0.

(3) The AFM results also indicated that sulfur-rich film was formed on the bornite surface at high anodic potential, making the surface thicker and rougher. Additionally, 400 mV was the most beneficial potential of bornite (bio)leaching.

Acknowledgments

The authors are grateful for the financial supports from the National Key Research and Development Program of China (Nos. 2022YFC2105300, 2022YFC2105304).

References

[1] TABELIN C B, PARK I, PHENGSAART T, JEON S, VILLACORTE-TABELIN M, ALONZO D, YOO K, ITO M, HIROYOSHI N. Copper and critical metals production from porphyry ores and E-wastes: A review of resource availability, processing/recycling challenges, socio-environmental aspects, and sustainability issues [J]. Resources, Conservation and Recycling, 2021, 170: 105610.

[2] HONG Mao-xin, HUANG Xiao-tao, GAN Xiao-wen, QIU Guan-zhou, WANG Jun. The use of pyrite to control redox potential to enhance chalcopyrite bioleaching in the presence of *Leptospirillum ferriphilum* [J]. Minerals Engineering, 2021, 172: 107145.

[3] ZHAO Chun-xiao, YANG Bao-jun, WANG Xing-xing, ZHAO Hong-bo, GAN Min, QIU Guan-zhou, WANG Jun. Catalytic effect of visible light and Cd^{2+} on chalcopyrite bioleaching [J]. Transactions of Nonferrous Metals Society of China, 2020, 30: 1078−1090.

[4] YANG Bao-jun, LUO Wen, LIAO Qi, ZHU Jian-yu, GAN Min, LIU Xue-duan, QIU Guan-zhou. Photogenerated-hole scavenger for enhancing photocatalytic chalcopyrite bioleaching [J]. Transactions of Nonferrous Metals Society of China, 2020, 30: 200−211.

[5] LIAO Rui, WANG Xing-xing, YANG Bao-jun, HONG Mao-xin, ZHAO Hong-bo, WANG Jun, QIU Guan-zhou. Catalytic effect of silver-bearing solid waste on chalcopyrite bioleaching: A kinetic study [J]. Journal of Central South University, 2020, 27: 1395−1403.

[6] LIAO Rui, YU Shi-chao, WU Bai-qiang, ZHAO Chun-xiao, LIN Hao, HONG Mao-xin, WU Hai-yan, YANG Cong-ren, ZHANG Yan-sheng, XIE Jian-ping, QIN Wen-qing, WANG Jun, QIU Guan-zhou. Sulfide mineral bioleaching: Understanding of microbe-chemistry assisted hydro-metallurgy technology and acid mine drainage environment protection [J]. Journal of Central South University, 2020, 27: 1367−1372.

[7] WANG Jun, QIN Wen-qing, ZHANG Yan-sheng, YANG Cong-ren. Bacterial leaching of chalcopyrite and bornite with native bioleaching microorganism [J]. Transactions of Nonferrous Metals Society of China, 2008, 18: 1468−1472.

[8] CHANG Ke-xin, ZHANG Yan-sheng, ZHANG Jia-ming, LI Teng-fei, WANG Jun, QIN Wen-qing. Effect of temperature-induced phase transitions on bioleaching of chalcopyrite [J]. Transactions of Nonferrous Metals Society of China, 2019, 29: 2183−2191.

[9] SILLITOE R H. Porphyry copper systems [J]. Economic Geology, 2010, 105: 3−41.

[10] PESIC B, OLSON F A. Dissolution of bornite in sulfuric acid using oxygen as oxidant [J]. Hydrometallurgy, 1984, 12: 195−215.

[11] PRICE D C, CHILTON J P. The anodic reactions of bornite in sulphuric acid solution [J]. Hydrometallurgy, 1981, 7: 117−133.

[12] YANG Cong-ren, JIAO Fen, QIN Wen-qing. Cu-state evolution during leaching of bornite at 50 °C [J]. Transactions of Nonferrous Metals Society of China, 2018, 28: 1632−1639.

[13] NYEMBWE K J, FOSSO-KANKEU E, WAANDERS F, MKANDAWIRE M. pH-dependent leaching mechanism of carbonatitic chalcopyrite in ferric sulfate solution [J]. Transactions of Nonferrous Metals Society of China, 2021, 31: 2139−2152.

[14] HONG Mao-xin, WANG Xing-xing, WU Ling-bo, FANG Chao-jun, HUANG Xiao-tao, LIAO Rui, ZHAO Hong-bo, QIU Guan-zhou, WANG Jun. Intermediates transformation of bornite bioleaching by *Leptospirillum ferriphilum* and *Acidithiobacillus caldus* [J]. Minerals, 2019, 9(3): 159.

[15] CAO Li-bo, HUANG Zhi-hua, SUN Xin, JIN Kai, CHANG Ke-xin, QIN Wen-qing, QIU Guan-zhou, WANG Jun, ZHANG Yan-sheng. Comparison of leaching of bornite from different regions mediated by mixed moderately thermophilic bacteria [J]. Journal of Central South University, 2020, 27: 1373−1385.

[16] WANG Xing-xing, LIAO Rui, ZHAO Hong-bo, HONG Mao-xin, HUANG Xiao-tao, PENG Hong, WEN Wen, QIN Wen-qing, QIU Guan-zhou, HUANG Cao-ming, WANG Jun. Synergetic effect of pyrite on strengthening bornite bioleaching by *Leptospirillum ferriphilum* [J]. Hydrometallurgy, 2018, 176: 9−16.

[17] BEVILAQUA D, ACCIARI H A, ARENA F A, BENEDETTI A V, FUGIVARA C S, FILHO G T, JNIOR O G. Utilization of electrochemical impedance spectro-scopy for monitoring bornite (Cu_5FeS_4) oxidation by

Acidithiobacillus ferrooxidans [J]. Minerals Engineering, 2009, 22: 254−262.

[18] BEVILAQUA D, ACCIARI H A, BENEDETTI A V, FUGIVARA C S, TREMILIOSI FILHO G, GARCIA O. Electrochemical noise analysis of bioleaching of bornite (Cu_5FeS_4) by *Acidithiobacillus ferrooxidans* [J]. Hydrometallurgy, 2006, 83: 50−54.

[19] ZHAO Hong-bo, HUANG Xiao-tao, HU Ming-hao, ZHANG Chen-yang, ZHANG Yan-sheng, WANG Jun, QIN Wen-qing, QIU Guan-zhou. Insights into the surface transformation and electrochemical dissolution process of bornite in bioleaching [J]. Minerals, 2018, 8: 173.

[20] TIAN Zu-yuan, LI Hao-dong, WEI Qian, QIN Wen-qing, YANG Cong-ren. Effects of redox potential on chalcopyrite leaching: An overview [J]. Minerals Engineering, 2021, 172: 107135.

[21] YANG Bao-jun, LIN Mo, FANG Jing-hua, ZHANG Rui-yong, LUO Wen, WANG Xing-xing, LIAO Rui, WU Bai-qiang, WANG Jun, GAN Min, LIU Bin, ZHANG Yi, LIU Xue-duan, QIN Wen-qing, QIU Guan-zhou. Combined effects of jarosite and visible light on chalcopyrite dissolution mediated by *Acidithiobacillus ferrooxidans* [J]. Science of the Total Environment, 2020, 698: 134175.

[22] SILVERMAN M P, LUNDGREN D G. Studies on the chemoautotrophic iron bacterium *Ferrobacillus ferrooxidans* I. An improved medium and a harvesting procedure for securing high cell yields [J]. Journal of Bacteriology, 1959, 77: 642−647.

[23] QUATRINI R, JOHNSON D B. *Acidithiobacillus ferrooxidans* [J]. Trends in Microbiology, 2019, 27: 282−283.

[24] YANG Bao-jun, ZHAO Chun-xiao, LUO Wen, LIAO Rui, GAN Min, WANG Jun, LIU Xue-duan, QIU Guan-zhou. Catalytic effect of silver on copper release from chalcopyrite mediated by *Acidithiobacillus ferrooxidans* [J]. Journal of Hazardous Materials, 2020, 392: 122290.

[25] YANG Bao-jun, LUO Wen, WANG Xing-xing, YU Shi-chao, GAN Min, WANG Jun, LIU Xue-duan, QIU Guan-zhou. The use of biochar for controlling acid mine drainage through the inhibition of chalcopyrite biodissolution [J]. Science of the Total Environment, 2020, 737: 139485.

[26] KHEZRI M, REZAI B, ABDOLLAHZADEH A A, WILSON B P, MOLAEINASAB M, LUNDSTRÖM M. Cyclic voltammetry and potentiodynamic polarization studies of chalcopyrite concentrate in glycine medium [J]. Transactions of Nonferrous Metals Society of China, 2021, 31: 545−554.

[27] MAJUSTE D, CIMINELLI V S T, OSSEO-ASARE K, DANTAS M S S, MAGALHÃES-PANIAGO R. Electrochemical dissolution of chalcopyrite: Detection of bornite by synchrotron small angle X-ray diffraction and its correlation with the hindered dissolution process [J]. Hydrometallurgy, 2012, 111/112: 114−123.

[28] ZHAO Hong-bo, WANG Jun, HU Ming-hao, QIN Wen-qing, ZHANG Yan-sheng, QIU Guan-zhou. Synergistic bioleaching of chalcopyrite and bornite in the presence of *Acidithiobacillus ferrooxidans* [J]. Bioresource Technology, 2013, 149: 71−76.

[29] AFFOUNE A M, SAILA A, BOUTEILLON J, POIGNET J C. Electrochemical behaviour of silver and rhenium electrodes in molten alkali fluorides [J]. Journal of Applied Electrochemistry, 2007, 37: 155−160.

[30] ZHAO Hong-bo, WANG Jun, QIN Wen-qing, HU Ming-hao, ZHU Shan, QIU Guan-zhou. Electrochemical dissolution process of chalcopyrite in the presence of mesophilic microorganisms [J]. Minerals Engineering, 2015, 71: 159−169.

[31] HIROYOSHI N, KUROIWA S, MIKI H, TSUNEKAWA M, HIRAJIMA T. Synergistic effect of cupric and ferrous ions on active-passive behavior in anodic dissolution of chalcopyrite in sulfuric acid solutions [J]. Hydrometallurgy, 2004, 74: 103−116.

[32] HONG Mao-xin, WANG Wei, LI Lai-shun, LIU Yang, TONG Li-zhi, QIU Guan-zhou, YANG Bao-jun, WANG Jun. The use of biogenic Fe^{3+} and H_2SO_4 generated from pyrite waste to enhance bornite bioleaching: A potential utilization of acid mine drainage [J]. Minerals Engineering, 2022, 190: 107927.

[33] ZHAO Hong-bo, HU Ming-hao, LI Yi-ni, ZHU Shan, QIN Wen-qing, QIU Guan-zhou, WANG Jun. Comparison of electrochemical dissolution of chalcopyrite and bornite in acid culture medium [J]. Transactions of Nonferrous Metals Society of China, 2015, 25: 303−313.

[34] HONG Mao-xin, WANG Xing-xing, YANG Bao-jun, LIU Shi-tong, LIN Hao, QIU Guan-zhou, QIN Wen-qing, WANG Jun. Effect of pyrite with different semiconducting properties on bornite bioleaching in the presence of *Leptospirillum ferriphilum* [J]. Hydrometallurgy, 2020, 196: 105414.

[35] BEVILAQUA D, DIÊZ-PEREZ I, FUGIVARA C S, SANZ F, GARCIA O Jr, BENEDETTI A V. Characterization of bornite (Cu5FeS4) electrodes in the presence of the bacterium *Acidithiobacillus ferrooxidans* [J]. Journal of the Brazilian Chemical Society, 2003, 14: 637−644.

[36] LISDAT F, SCHAFER D. The use of electrochemical impedance spectroscopy for biosensing [J]. Analytical and Bioanalytical Chemistry, 2008, 391: 1555−1567.

[37] TU Zhi-hong, WAN Jing-jing, GUO Chu-ling, FAN Cong, ZHANG Ting, LU Gui-ning, REINFELDER J R, DANG Zhi. Electrochemical oxidation of pyrite in pH 2 electrolyte [J]. Electrochimica Acta, 2017, 239: 25−35.

[38] LIU Shi-tong, HONG Mao-xin, WANG Xing-xing, YANG Bao-jun, LIN Hao, LIN Mo, WANG Jun, QIU Guan-zhou. Pretreatment with acidic ferric sulfate leaching promotes the bioleaching of bornite [J]. Hydrometallurgy, 2020, 196: 105349.

[39] LI Y, KAWASHIMA N, LI J, CHANDRA A P, GERSON A R. A review of the structure, and fundamental mechanisms and kinetics of the leaching of chalcopyrite [J]. Advances in Colloid and Interface Science, 2013, 197/198: 1−32.

[40] GHAHREMANINEZHAD A, DIXON D G, ASSELIN E. Electrochemical and XPS analysis of chalcopyrite ($CuFeS_2$) dissolution in sulfuric acid solution [J]. Electrochimica Acta, 2013, 87: 97−112.

[41] GOH S W, BUCKLEY A N, LAMB R N, ROSENBERG R A, MORAN D M. The oxidation states of copper and iron in mineral sulfides, and the oxides formed on initial exposure of

chalcopyrite and bornite to air [J]. Geochimica Et Cosmochimica Acta, 2006, 70: 2210−2228.

[42] GHAHREMANINEZHAD A, ASSELIN E, DIXON D G. Electrodeposition and growth mechanism of copper sulfide nanowires [J]. The Journal of Physical Chemistry C, 2011, 115: 9320−9334.

[43] XIA Jin-lan, SONG Jian-jun, LIU Hong-chang, NIE Zhen-yuan, SHEN Li, YUAN Peng, MA Chen-yan, ZHENG Lei, ZHAO Yi-dong. Study on catalytic mechanism of silver ions in bioleaching of chalcopyrite by SR-XRD and XANES [J]. Hydrometallurgy, 2018, 180: 26−35.

[44] YANG Con-gren, JIAO Fen, QIN Wen-qing. Co-bioleaching of chalcopyrite and silver-bearing bornite in a mixed moderately thermophilic culture [J]. Minerals, 2017, 8: 4.

[45] ZHAO Chun-xiao, YANG Bao-jun, LIAO Rui, HONG Mao-xin, YU Shi-chao, WANG Jun, QIU Guan-zhou. Catalytic mechanism of manganese ions and visible light on chalcopyrite bioleaching in the presence of *Acidithiobacillus ferrooxidans* [J]. Chinese Journal of Chemical Engineering, 2022, 41: 457−465.

[46] ZHAO Chun-xiao, YANG Bao-jun, LIAO Rui, HONG Mao-xin, YU Shi-chao, LIU Shi-tong, WANG Jun, QIU Guan-zhou. Combined effect and mechanism of visible light and Ag^+ on chalcopyrite bioleaching [J]. Minerals Engineering, 2022, 175: 107283.

[47] GAO Kun, HU Yue, GUO Chu-ling, KE Chang-dong, LU Gui-ning, DANG Zhi. Mobilization of arsenic during reductive dissolution of As(V)-bearing jarosite by a sulfate reducing bacterium [J]. Journal of Hazardous Materials, 2021, 402: 123717.

[48] HONG Mao-xin, LIU Shi-tong, HUANG Xiao-tao, YANG Bao-jun, ZHAO Chun-xiao, YU Shi-chao, LIU Yu-ling, QIU Guan-zhou, WANG Jun. A review on bornite (bio)leaching [J]. Minerals Engineering, 2021, 174: 107245.

[49] HUANG Xiao-tao, LIAO Rui, YANG Bao-jun, YU Shi-chao, WU Bai-qiang, HONG Mao-xin, WANG Jun, ZHAO Hong-bo, GAN Min, JIAO Fen, QIN Wen-qing, QIU Guan-zhou. Role and maintenance of redox potential on chalcopyrite biohydrometallurgy: An overview [J]. Journal of Central South University, 2020, 27: 1351−1366.

[50] SUN Xin, YUAN Wen-bing, JIN Kai, ZHANG Yan-sheng. Control of the redox potential by microcontroller technology: Researching the leaching of chalcopyrite [J]. Minerals, 2021, 11: 382.

斑铜矿在电化学溶解过程中表面钝化物的演变

洪茂鑫[1,2]，林 豪[1,2]，杨宝军[1,2]，肖 婧[1]，廖 狴[1,2]，
于世超[1,2]，赵春晓[1,2]，刘仕统[1,2]， 孙 欣[1,2]，王 军[1,2]，邱冠周[1,2]

1. 中南大学 资源加工与生物工程学院，长沙 410083；
2. 中南大学 生物冶金教育部重点实验室，长沙 410083

摘 要：在斑铜矿(生物)浸出过程中，中间产物的产生与氧化还原电位之间的关系尚不清楚。本文作者采用一系列电化学试验和表面分析方法研究天然斑铜矿的电化学溶解行为和表面硫物种的形成。电化学试验表明，在宽阳极电位下(300~800 mV(vs Ag/AgCl))，斑铜矿电极表面经历 3 种不同的变化，即“活化”(<400 mV(vs Ag/AgCl))，“钝化”(400~700 mV(vs Ag/AgCl))和 “过钝化”(>700 mV(vs Ag/AgCl))。XPS 结果表明，在斑铜矿电化学溶解过程中表面产生的含硫中间产物包括类铜蓝、S_n^{2-}/S^0 和不溶性 SO_4^{2-}。此外，原子力显微镜结果证实：当施加的电位分别为 600 和 700 mV(vs Ag/AgCl)时，由于 S_n^{2-}/S^0 的积累，斑铜矿表面会受到严重钝化。斑铜矿(生物)浸出最有利的电位为 400 mV (vs Ag/AgCl)。

关键词：斑铜矿；生物浸出；电化学溶解；表面物种；原子力显微镜

(Edited by Wei-ping CHEN)